Workability Behavior of Powder Metallurgy Carbide Reinforced Aluminum Composites during Hot Forging

DOI: 10.1080/10426914.2015.1004703

Sumesh Narayan[a*] & Ananthanarayanan Rajeshkannan[a*]

Abstract

Experimental study was conducted to assess the consequence of titanium carbide (TiC), molybdenum carbide (Mo_2C), iron carbide (Fe_3C) and tungsten carbide (WC) reinforcements on the composite aluminium compacts. The hot deformation of the carbide reinforce aluminium compacts, Al-2TiC, Al-2WC, Al-2Fe_3C and Al-2Mo_2C, with aspect ratios (AR) of 0.4 and 0.6, was carried out and the workability behavior of the same was determined. The effect of carbide reinforcement and preform geometry on the relative density, stress ratio, $\sigma_\theta/\sigma_{eff}$, and formability ratio was studied.

WORKABILITY BEHAVIOR OF POWDER METALLURGY CARBIDE REINFORCED ALUMINUM COMPOSITES DURING HOT FORGING

Sumesh Narayan[1, a], Ananthanarayanan Rajeshkannan[1, b]

[1]Section of Mechanical Engineering, FSTE, USP, Suva, Fiji.

[a]Corresponding Author: email: narayan_su@usp.ac.fj or kesh_ria@yahoo.com,

phone - +679 3232034

[b]narayanan_a@usp.ac.fj

Abstract

Experimental study was conducted to assess the consequence of titanium carbide (TiC), molybdenum carbide (Mo_2C), iron carbide (Fe_3C) and tungsten carbide (WC) reinforcements on the composite aluminium compacts. The hot deformation of the carbide reinforce aluminium compacts, Al-2TiC, Al-2WC, Al-2Fe_3C and Al-2Mo_2C, with aspect ratios (AR) of 0.4 and 0.6, was carried out and the workability behavior of the same was determined. The effect of carbide reinforcement and preform geometry on the relative density, stress ratio, $\sigma_\theta / \sigma_{eff}$, and formability ratio was studied.

Keywords:

Formability; Powder metallurgy; Carbide.

1. Introduction

One of the fundamental quests today is to produce parts using green manufacturing technology. Powder metallurgy (PM) process is considered to be green manufacturing as PM process releases very little fumes and chemicals in the atmosphere. Further, energy consumption can be reduced up to 50% in comparison to traditional casting manufacturing route [1]. PM is near net shape production technology and hence, there is no wastage or raw materials in comparison to other manufacturing route. Parts requiring control porosity such as filter materials can be produced by PM manufacturing route. Apart from many merits of this PM route, one of the major drawbacks of this process is the remaining porosity in the compacts after the primary PM process, blending/mixing, compaction and sintering process. Hence, for high

strength industrial applications the compacts needs to further go through the additional processes such as pressing, infiltration, powder rolling and extrusion to improve its mechanical properties [2].

The major concern in secondary compression is to attain the required shape without any failure of the work part. Workability is the extent of deformation of a material prior to failure and is affected by several parameters such as temperature, strain rate, preform shape, material composition and initial relative density [3]. Several constitutive equations have been developed to study workability characteristics of PM materials [4-6]. A new yield criterion was developed by Doraivelu et al. [7], which was further modified by Raj et al. [2] under different stress state conditions. Lin et al. [8, 9] proposed another form of the yield criterion using some plastic constitutive equation for PM materials. Rajeshkannan [10] showed smaller height to diameter ratio compacts showed constant densification because of quick stress transfer between powder particles causing excessive matrix and geometric hardening. Bao [11] published a correlation between two important parameters, stress triaxiality and effective strain to study the failure of PM materials, that is, development of crack during deformation. Rajeshkannan et al. [12] reported the consequence of strains such as true height strain, effective strain and true hoop strain on the bulged surface prone to failure by crack formation. Further, respective stresses during upsetting on PM compacts were determined. Kumar et al. [13] investigated the ductile rupture in metal upsetting experimentally and validated it using theoretical models. They showed some of the significant criterions normally employed for the prediction of ductile rupture. Several researchers used finite element method to determine the start of crack formation site and the extent of upsetting at which the crack will occur [14, 15]. One of the important parameters to study during the workability studies is the formability ratio developed by Rahman and El-Sheikh [5]. The formability ratio describes the consequence of hydrostatic stress and equivalent stress and the mathematical equation of the same is given by Raj et al. [2]. Many researchers [16, 17] have worked and evaluated the forming limit of PM materials and used the analysis in preform shape design and die constraints designs. These are important as to arrest cracks before it appears on the free surface during the forming process.

Hard carbide particles addition in aluminium metal matrix composites provides an opportunity to improve mechanical properties, wear resistance and corrosion resistance. Even though many literature deals with silicon carbides based aluminium composites, the full analysis such as mechanical properties, microstructure, workability, fractography are not attempted via hot deformation. Further, little work has been attempted via hot deformation on titanium carbide, tungsten carbide, iron carbide and molybdenum carbide to understand its behavior [18-21]. Thus, the current research is intended to study the workability limit of PM compacts of Al-2TiC, Al-2WC, Al-2Fe_3C, and Al-2Mo_2C (weight percentage) experimentally. The topic selected by the authors is of great significance for industries such as automobile aerospace and many others.

2. Materials and Method

Carbide reinforced aluminium metal matrix composites are widely used in high strength industrial application due to low specific density, good wear resistance and low thermal expansion coefficient. Thus in the present research several carbides are used to manufacture parts with new material combinations. Aluminium powder of less than or equal to 150 μm and respective carbide powders, namely, titanium carbide, tungsten carbide, molybdenum carbide and iron carbide, of less than or equal to 50 μm were mixed to obtain Al-2TiC, Al-2WC, Al-2Fe_3C and Al-2Mo_2C through ball milling. The ball mill was run for 2 hours at 200 rpm to get a homogenized mixture. The apparent density was continuously measured to ensure homogenous mixture was obtained. The sieve analysis of pure aluminium powder and powder characterization of aluminium powder and its respective blends are given in Tables 1 and 2, respectively.

Table 1. Sieve size breakdown of pure aluminium powder

Sieve size (µm)	250	+200	+150	+100	+75	+45	-45
Wt % Ret.	0.2	0.3	16.3	55.3	9.5	7.9	10.5

Table 2. Characterization of aluminium powder and its blends

Property	Al	Al-2WC	Al-2TiC	Al-2Fe_3C	Al-2Mo_2C
Apparent Density (g/cc)	1.091	1.262	1.186	1.236	1.258

Flow rate, (s/50g)	87.306	78.848	85.202	78.909	78.132
Compressibility (g/cc) at pressure of 130±10MPa	2.356	2.273	2.325	2.313	2.301

The powders corresponding to height-to diameter ratios (AR) of 0.4 and 0.6 were compacted in a pressure range of 139MPa to 159MPa (hydraulic press) to obtain relative density of 0.86 ± 0.01. The respective compacting pressures were obtained from the compressibility curve prepared for each material. The preforms were covered with ceramic coating (Al_2O_3 mixed with acetone) to avoid oxidation during the sintering process. Firstly, the compacts were coated on all surfaces with ceramic coating. This coating was allowed to dry for a period 12 hours at normal atmospheric conditions. Recoating was employed to the preforms in the direction 90^o to that of the earlier coating. Again the compacts were allowed to dry for a period of 12 hours.

The ceramic covered compacts were further dried in an electric muffle furnace at 220^oC for 30 minutes (drying process) and then the temperature was increased to 594^oC. At 594^oC the preforms were sintered for an additional period of 60 minutes. Each perform was compressively deformed at a temperature of 594^oC (sintering temperature) to different levels of axial strain. The following measurements of the forged compacts were taken, forged height and forged compact diameters (top surface, bottom surface and bulged diameter). Further, relative densities of all the compacts were measured using Archimedes principle. Experimental data's were used to compute the stress ratio parameter, $\sigma_\theta / \sigma_{eff}$, axial strain, true diameter strain, percent relative density, actual bulged length and formability ratio.

3. Theoretical analysis under triaxial stress state conditions

According to Abdel-Rahman and El-Sheikh [5], axial strain and axial stress can be calculated from the following equations:

$$\varepsilon_z = \ln\left(\frac{h_f}{h_o}\right) \tag{1}$$

$$\sigma_z = \frac{load}{contact\ \ surface\ \ area} \tag{2}$$

and true hoop strain is

$$\varepsilon_\theta = \varepsilon_r = \ln\left(\frac{D_f}{D_o}\right) \tag{3}$$

Raj et al. [2] presented the hoop strain which includes the forged bulged diameter (D_b) and forged contact diameter (D_c) can be expressed as follows

$$\varepsilon_\theta = \ln\left[\frac{2D_b^2 + D_c^2}{3D_o^2}\right] \tag{4}$$

Kumar et al. [13] presented the state of stress as:

$$\alpha = \frac{d\varepsilon_\theta}{d\varepsilon_z} = \frac{(2+R^2)\sigma_\theta - R^2(\sigma_z + 2\sigma_\theta)}{(2+R^2)\sigma_z - R^2(\sigma_z + 2\sigma_\theta)} \tag{5}$$

When α, R and σ_z are known, Eq. (5) can be used to calculate the hoop stress (σ_θ) as:

$$\sigma_\theta = \left[\frac{2\alpha + R^2}{2 - R^2 + 2R^2\alpha}\right]\sigma_z \qquad (\text{where, } \alpha = \frac{d\varepsilon_\theta}{d\varepsilon_z}) \tag{6}$$

Further, rearranging Equation 6

$$\frac{\sigma_\theta}{\sigma_z} = \left[\frac{2\alpha + R^2}{2 - R^2 + 2R^2\alpha}\right] \tag{7}$$

Using cylindrical coordinates ($\sigma_\theta = \sigma_r$), the hydrostatic stress is calculated as:

$$\sigma_m = \frac{\sigma_r + \sigma_\theta + \sigma_z}{3} = \frac{2\sigma_\theta + \sigma_z}{3} \tag{8}$$

Further, rearranging Equation 8

$$\frac{\sigma_m}{\sigma_z} = \frac{1}{3}\left(1 + \frac{2\sigma_\theta}{\sigma_z}\right) \tag{9}$$

Doraivelu et al. [7] presented the equation of the effective stress as:

$$\sigma_1^2 + \sigma_2^2 + \sigma_3^2 - R^2(\sigma_1\sigma_2 + \sigma_2\sigma_3 + \sigma_3\sigma_1) = \sigma_{eff}^2 (2R^2 - 1) \quad (10)$$

Equation 10 in cylindrical coordinates for cylindrical axisymmetric upsetting ($\sigma_\theta = \sigma_r$) can be written as

$$\sigma_z^2 + 2\sigma_\theta^2 - R^2(\sigma_\theta^2 + 2\sigma_\theta\sigma_z) = \sigma_{eff}^2 (2R^2 - 1) \quad (11)$$

Rearranging equation 11

$$\frac{\sigma_{eff}}{\sigma_z} = \left[\frac{1 + 2(\sigma_\theta / \sigma_z)^2 - R^2(2(\sigma_\theta / \sigma_z) + (\sigma_\theta / \sigma_z)^2)}{2R^2 - 1}\right]^{0.5} \quad (12)$$

Vujovic and Shabaik [4] proposed the formability ratio as:

$$\beta = 3\left[\frac{(\sigma_m / \sigma_z)}{(\sigma_{eff} / \sigma_z)}\right] \quad (13)$$

Equation (13) gives the influence of hydrostatic stress and equivalent stress during the forging operation of PM preforms.

4. Results and discussion

Figure 1 gives R vs ε_z for AR of 0.40 and 0.60, these plots being drawn for initial relative density of 86%. As seen in Fig. 1 the relative density increases up to 0.45 axial strain and thereafter relative density is almost constant till fracture strain. Lower AR preforms showed better densification in comparison to higher AR compacts because of the existence of smaller number of pores in the smaller AR preforms. TiC reinforced aluminium showed better densification rate and better final density achieved followed by Fe_3C reinforced aluminium and then Mo_2C reinforced aluminium. WC reinforced aluminium had the lowest densification rate and final density achieved. However, an inverse relationship exists between densification and fracture strain for the respective composites. Further, Fig. 2 gives variation of lateral strain and axial strain for AR of 0.40 and 0.60, these plots being drawn for starting relative density of 86%. As seen in Fig. 2 the lateral deformation is highest in WC reinforced aluminium composite followed by Mo_2C, then Fe_3C and then TiC composites. This means the effective closer of pores is higher in TiC reinforced aluminium, therefore, it has higher density than any other composite tested. Firstly,

the smaller pores present at the center of the preform are eliminated effectively during the deformation process. Secondly, the cylindrical shaped pores and pores towards the side of the preform are extensively elongated and then closed due to the lateral flow of the material during deformation. The second mechanism of pore closure is more in WC reinforced aluminium; hence, it showed lower densification.

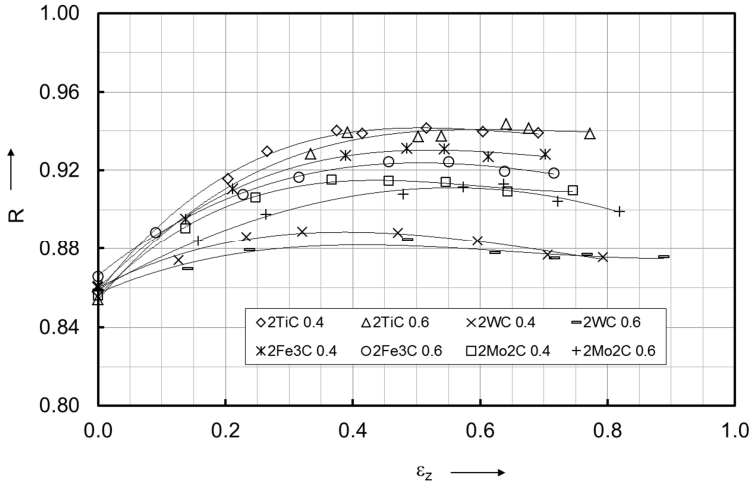

Fig. 1: R vs ε_z during hot deformation.

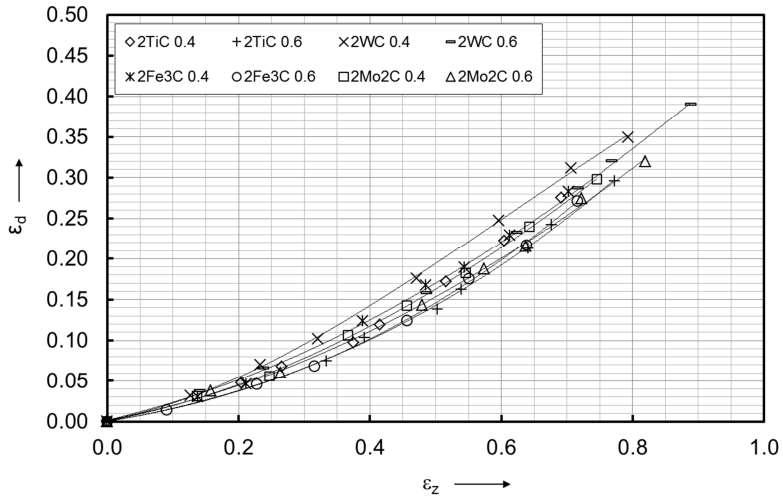

Figure 2: The variation of the diameter strain against axial strain during hot deformation.

Figure 3 gives $\sigma_\theta / \sigma_{eff}$ vs R for AR of 0.40 and 0.60, these plots being drawn for initial relative density of 86%. From Fig. 3 it can be seen that the influence of AR and composition is nil on the characteristics behavior. The hoop stress increase as the relative density increase. The rate, at which the hoop stress increase, increases as the

densification progresses and the final stress ratio and relative density achieved at the end of deformation is different for the respective composition. Against densification, the highest hoop stress value was achieved by TiC content composite followed by Fe_3C composite, Mo_2C composite and lowest was WC containing composite. Further, the highest hoop stress was obtained for smaller aspect ratio preform. This indicates that WC containing composite and higher AR preform has further chance to be deformed if the preform is free of cracks. The lateral deformation at the contact surface is lowest in TiC composite as seen in Fig. 2 for any given axial strain indicating the bulging phenomenon is highest in TiC composite compared to Fe_3C, Mo_2C, and WC composites. Hence, the hoop stress is found to be highest in TiC composite compared to other composites. A very similar behavior is found for mean stress and axial stress (graphs not plotted here).

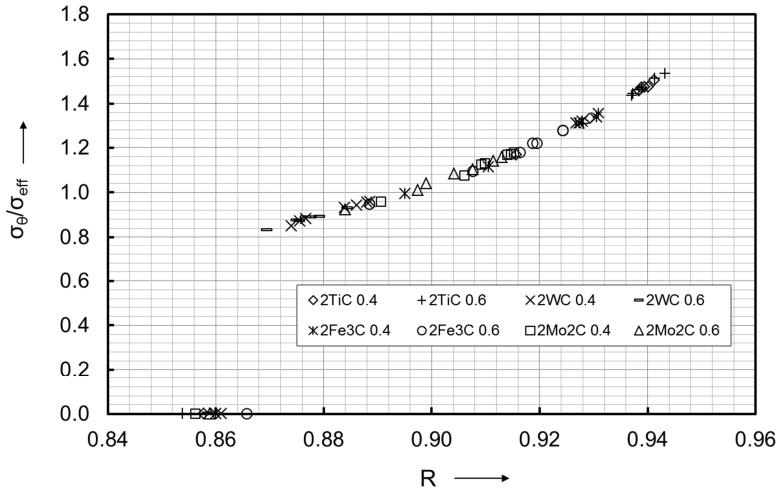

Figure 3: Relationship between hoop stress ($\sigma_\theta / \sigma_{eff}$) and relative density during hot deformation.

Figure 4 gives $\sigma_\theta / \sigma_{eff}$ vs ε_z for AR of 0.40 and 0.60, these plots being drawn for starting theoretical density of 86%. The influence of AR on hoop stress is literally nil, especially towards the end of deformation when plotted against axial strain. The hoop stress rises to a maximum value as the deformation starts and then settles for the steady state stress for the rest for the deformation. For any given axial strain, the hoop stress obtained is highest for TiC containing compacts, followed by Fe_3C, Mo_2C and lowest for WC containing compacts. This means WC containing compacts can be further deformed provided it is free from defects. The TiC particulates resists the motion of dislocations more than Fe_3C, Mo_2C and WC particulates and hereafter the

load application for further deformation for TiC composite is more than other composite. Due to this reason the hoop stress is higher for TiC composite for any given axial strain. A very similar behavior is found for mean stress and axial stress (graphs not plotted here).

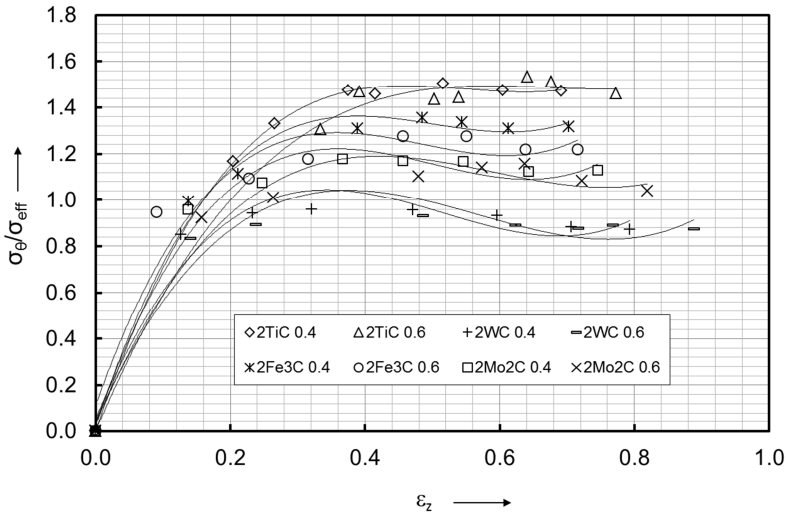

Fig. 4: $\sigma_\theta / \sigma_{eff}$ vs ε_z during hot deformation.

Figure 5 shows formability stress ratio, β, against axial strain for AR of 0.40 and 0.60, these plots being drawn for starting relative density of 86%. The formability of the TiC containing compacts was found to be higher followed by Fe_3C and Mo_2C composites. WC containing compacts showed lowest formability ratio for any given axial strain. For any given axial strain, the *R* is found to be highest in TiC composite, Fig. 1, meaning the porosity level is low and hence the reason for high formability ratio for TiC composite. Further, the hoop stress is higher in TiC composite than the true effective stress compared to Fe_3C, Mo_2C and WC composite (Fig. 3) is the reason for high formability in TiC composite. The compositions are calculated using weight percentage and TiC particulate being the lowest weight followed by Fe_3C, Mo_2C and WC (Table 2). This means the amount of smaller and fine pores present in Al-2TiC composite is more than other composite. The effective closure of pores is more in TiC composite increasing the densification (Fig. 1) and hence, for the same reason the formability ratio is higher in TiC composite. Further, Fig. 6 shows formability stress ratio against *R* for AR of 0.40 and 0.60, these plots being drawn for starting relative density of 86%. The effect of AR and composition showed nil effect on the

formability behavior against relative density, however, the final formability ratio achieved against density and axial strain is also important. In view of this a graph of formability ratio at fracture and fracture strain is plotted as shown in Fig. 7. The axial strain at fracture is found to be higher for higher AR compacts in comparison to smaller AR preforms. There is an inverse relationship between fracture strain and fracture formability ratio as shown in Fig. 7. WC containing compacts showed higher fracture strain followed by Mo_2C composite, then Fe_3C composite and lowest fracture strain for TiC composites. Theses graphs are important and can be utilized in the preform shape and die constraint design.

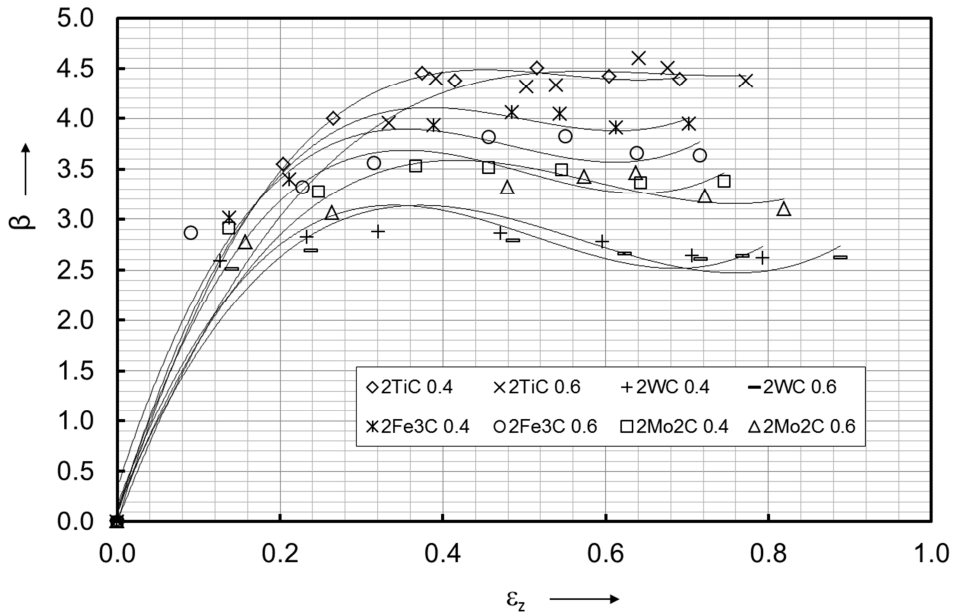

Figure 5: β vs ε_z during hot deformation.

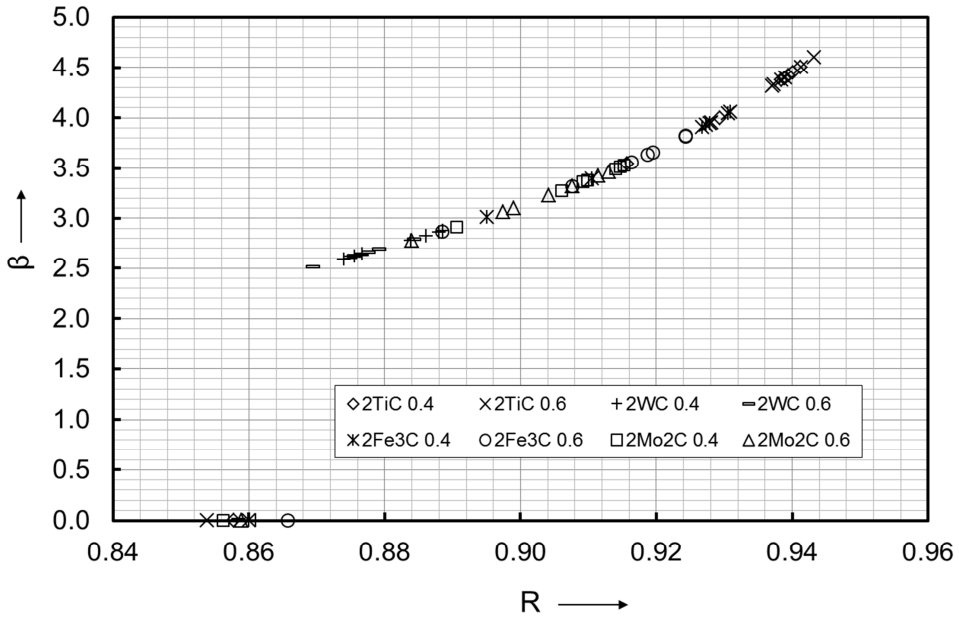

Figure 6: β vs R during hot deformation.

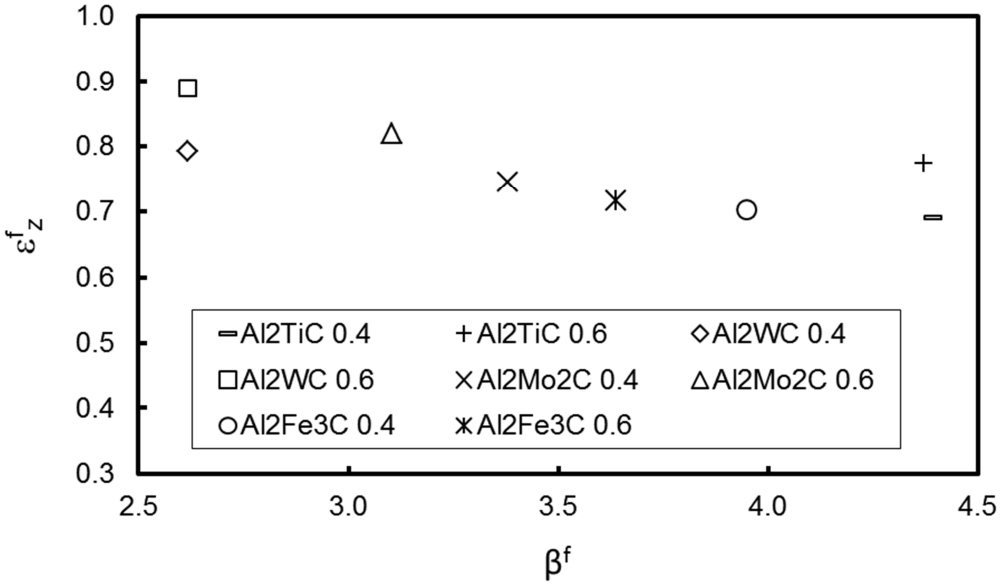

Figure 7: ε_z^f vs β^f during hot deformation.

Figure 8 show the optical micrographs of hot forged aluminium composites along the upsetting direction. It can be seen that the grains are deformed and elongated perpendicular to the compression direction (compression direction is horizontal in Fig. 8). The elongation of particles is more in WC, followed by Mo_2C, Fe_3C and lowest in TiC composite. The inter-particle spacing in TiC reinforced aluminium composite is small due to more TiC particles present then in Fe3C, Mo2C, and WC reinforced aluminium, respectively. Hence, the effective closure of pores is more in

Al-2TiC composite promoting densification and formability as seen in Figs. 1 and 5, respectively.

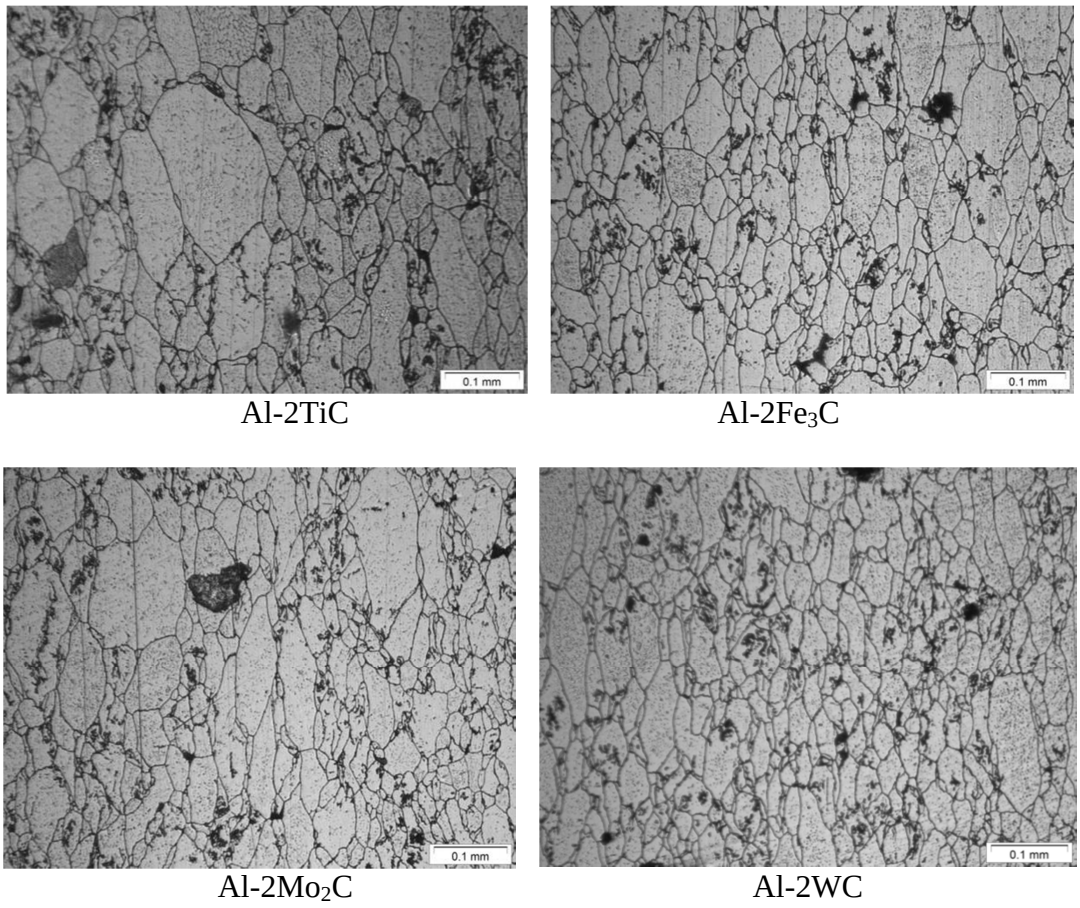

Al-2TiC Al-2Fe_3C

Al-2Mo_2C Al-2WC

Fig. 8: Optical micrographs of various sintered aluminium composites with 50% deformation at the center.

5. Conclusions

The design of preform shape and die are very important such that the final part produced is free from defects (fracture). Accordingly the following conclusions are made.

- The TiC containing compacts showed better densification rate thus better stress formability index of the preform followed by Fe_3C, then Mo_2C and lowest for WC containing compacts. However, TiC containing compacts gave lowest axial strain to fracture.
- Reducing the AR enables uniform deformation resulting in improved densification and formability behavior of the preform, however, limits the axial strain to fracture.

- The variation of aspect ratio and hard carbide particles in aluminium composite made nil impact in the stress ratio behavior against densification, however, against true axial strain induced is prominent.
- The grains and porosity are seen to be deformed and elongated perpendicular to the direction of compression.

References

[1] Mascarenhas, J. Powder Metallurgy: A major partner of sustainable development. *Material Science Forum* **2004**, *455-466*, 857-860.

[2] Raj, A.P.M.; Selvakumar, N.; Narayanasamy, R.; Kailasanathan, C. Experimental investigation on workability and strain hardening behaviour of Fe–C–Mn sintered composites with different percentage of carbon and manganese content. *Materials and Design* **2013**, *49*, 791-801.

[3] Taha, M.A.; El-Mahallawy, N.A.; El-Sabbagh, A.M. Some experimental data on workability of aluminium-particulate-reinforced metal matrix composites. *Journal of Materials Processing Technology* **2008**, *202*, 380-385.

[4] Vujovic, V.; Shabaik, A.H. A new workability criterian for ductile materials. *Journal of Engineering Materials and Technology* **1986**, *108*, 245-249.

[5] Rahman, M.A.; El-Sheikh, M.N. Workability in forging of powder metallurgy compacts. *Journal of Materials Processing Technology* **1995**, *54*, 97-102.

[6] Krishna, C.H.; Davidson, M.J.; Nagaraju, C. Utilization of workability criteria to improve the formability of the deformed truncated billets in simple upsetting. *Procedia Materials Science* **2014**, *5*, 1392-1397.

[7] Doraivelu, S.M. ; Gegel, H.L. ; Gunasekara, J.S. ; Malas, J.C. ; Morgan, J.T. A new yield function for compressible P/M materials. *International Journal of Mechanical Science* **1984**, *26*, 527–35.

[8] Hua, L.; Qin, X.; Mao, H.; Zhao, Y. Plastic yield deformation and yield criterion for compressible sintered powder materials. *Journal of Materials Processing Technology* **2006**, *180*, 174-178.

[9] Ko, B.C.; Park, G.S.; Yoo, Y.C. The effects of SiC particle volume fraction on the microstructure and hot workability of SiC_p/AA 2024 composite. *Journal of Materials Processing Technology* **1999**, *95*, 210-215.

[10] Rajeshkannan, A.; Narayan, S. Phenomenon of instantaneous work hardening characteristics of sintered cold deformed Cu alloy preforms. *Advanced Materials Research* **2013**, *651*, 295-301.

[11] Bao, Y. Dependence of ductile cracks formation in tensile tests on stress triaxiality stress and strain ratios. *Engineering Fracture Mechanics* **2005**, *72*, 505-522.

[12] Rajeshkannan, A.; Mehta, U. Deformation study of sintered iron–carbon–silicon–copper steel compacts during cold forging. *Materials and Manufacturing Processes* **2014**, *29*, 442-447.

[13] Kumar, D.R.; Narayanasamy, R.; Loganathan, C. Effect of Glass and SiC in Aluminum matrix on workability and strain hardening behavior of powder metallurgy hybrid composites. *Materials and Design* **2012**, *32*, 120-136.

[14] Saanouni, K. On the numerical prediction of the ductile fracture in metal forming. *Engineering Fracture Mechanics* **2008**, *75*, 3545-3559.

[15] Hoa, V.C.; Seo, D.W.; Lim, J.K. Site of ductile fracture initiation in cold forging: a finite element model. *Theoretical Applied Fracture Mechanics* **2005**, *44*, 58-69.

[16] Hassani, A.; Bagherpour, E.; Qods, F. Influence of pores on workability of porous Al/SiC composites fabricated through powder metallurgy + mechanical alloying. *Journal of Alloys and Compounds* **2014**, *591*, 132-142.

[17] Rajeshkannan, A.; Rengamani, D.S.; Sharma, A. Some aspects on geometric and matrix work-hardening characteristics of sintered cold forged copper alloy preforms. *Materials Research* **2014**, *17*, 196-202.

[18] Roshan, M.R.; Taherzadeh, R.M.; Ebrahimkhani, H.; Mosleh, A. Fabrication of Al-based composites reinforced with Al_2O_3-TiB_2 ceramic composite particulates using vortex-casting method. *Journal of Mining and Metallurgy B: Metallurgy* **2013**, *49*, 299-305.

[19] Izadi, H.; Nolting, A.; Munro, C.; Bishop, D.P.; Plucknett, K.P.; Gerlich, A.P. Friction stir processing of Al/SiC composites fabricated by powder metallurgy. *Journal of Materials Processing Technology* **2013**, *213*, 1900-1907.

[20] Kumar, A.; Mahapatra, M.M.; Jha, P.K. Fabrication and characterizations of mechanical properties of Al-4.5%Cu/10TiC composite by In-Situ method. *Journal of Minerals and Materials Characterization and Engineering* **2012**, *11*, 1075-1080.

[21] Lui, C.Y.; Wang, Q.; Jia, Y.Z.; Zhang, B.; Jing, R.; Ma, M.Z.; Jing, Q.; Lui, R.P. Evaluation of mechanical properties of 1060-Al reinforced with WC particles via warm accumulative roll bonding process. *Material Science Engineering A* **2013**, *43*, 367-372.

Notation

ε_θ	True hoop strain
ε_z	True axial strain
ε_z^f	True axial strain to fracture
ε_{eff}	Effective strain
σ_z	Axial stress
σ_θ	Hoop stress
σ_r	Radial stress
σ_m	Hydrostatic stress
σ_{eff}	Effective stress
β	Formability ratio
β^f	Formability ratio at fracture
R	Relative density
α	Poisson's ratio
$d\varepsilon_\theta$	Plastic hoop strain increment
$d\varepsilon_z$	Plastic axial strain increment
h_o	Initial height
h_f	Forged height
D_o	Initial diameter
D_f	Forged contact diameter